

## Article

# Conceptual Design and Aerostructural Trade-Offs in Hydrogen-Powered Strut-Braced Wing Aircraft: Insights into Dry and Wet Ultra-High Aspect Ratio Wings

Nicolas F. M. Wahler <sup>1,\*</sup>, Yiyuan Ma <sup>2</sup> and Ali Elham <sup>1</sup>

<sup>1</sup> Department of Aeronautics and Astronautics, University of Southampton, Burgess Road, Southampton SO16 7QF, UK; a.elham@soton.ac.uk

<sup>2</sup> Visionary Aircraft Concepts, Bauhaus Luftfahrt e.V., Willy-Messerschmitt-Straße 1, 82024 Taufkirchen, Germany; yiyuan\_ma@outlook.com

\* Correspondence: n.wahler@soton.ac.uk

**Abstract:** Stringent sustainability goals are set for the next generation of aircraft. A promising novel airframe concept is the ultra-high aspect ratio Strut-Braced Wing (SBW) aircraft. Hydrogen-based concepts are active contenders for sustainable propulsion. The study compares a medium-range Liquid Hydrogen (LH<sub>2</sub>) to a kerosene-based SBW aircraft designed with the same top-level requirements. For both concepts, overall design, operating costs, and emissions are evaluated using the tool SUAVE. Furthermore, aerostructural optimizations are performed for the wing mass of SBW aircraft with and without wing-based fuel tanks. Results show that the main difference in the design point definition results from a higher zero-lift drag due to an extended fuselage housing the LH<sub>2</sub> tanks, with a small reduction in the required wing loading. Structural mass increases of the LH<sub>2</sub> aircraft due to additional tanks and fuselage structure are mostly offset by fuel mass savings. While the fuel mass accounts for nearly 25% of the kerosene design's Maximum Take-Off Mass (MTOM), this reduces to 10% for the LH<sub>2</sub> design. The LH<sub>2</sub> aircraft has 16% higher operating costs with emission levels reduced to 57–82% of the kerosene aircraft, depending on the LH<sub>2</sub> production method. For static loads, the absence of fuel acting as bending moment relief in the wing results in an increase in wing structural mass. However, the inclusion of roll rate requirements causes large wing mass increases for both concepts, significantly outweighing dry wing penalties.

**Keywords:** strut-braced wing; hydrogen; ultra-high aspect ratio wing; aerostructural optimization; aircraft design



Academic Editor: Giacomo Silvagni

Received: 22 December 2024

Revised: 17 January 2025

Accepted: 20 January 2025

Published: 23 January 2025

**Citation:** Wahler, N.F.M.; Ma, Y.; Elham, A. Conceptual Design and Aerostructural Trade-Offs in Hydrogen-Powered Strut-Braced Wing Aircraft: Insights into Dry and Wet Ultra-High Aspect Ratio Wings. *Aerospace* **2025**, *12*, 77. <https://doi.org/10.3390/aerospace12020077>

**Copyright:** © 2025 by the authors. Licensee MDPI, Basel, Switzerland. This article is an open access article distributed under the terms and conditions of the Creative Commons Attribution (CC BY) license (<https://creativecommons.org/licenses/by/4.0/>).

## 1. Introduction

In an effort to increase the drive towards more sustainability in aviation, stringent sustainability goals have been set by the European Commission [1] and NASA [2] for the next generation of aircraft. With current aircraft and propulsion concepts reaching their respective performance limits, these goals require new approaches in both airframe and propulsion solutions. One promising airframe concept is the Ultra-High Aspect Ratio Wing (UHARW) [3]. For a given required wing area, the high aspect ratio and, hence, increased wingspan reduce induced drag and, therefore, increase fuel efficiency. However, the aerodynamic load also increases the wing bending moment and, hence, the structural mass of the wing, limiting the overall benefits. For medium-range designs, the mission fuel mass starts to increase exponentially when the wing aspect ratio exceeds 16 [4]. To counteract this,

the addition of a strut can reduce the bending moment by up to 50% [5]. Further benefits and wing weight reduction can be gained from advanced composite materials that allow aeroelastic tailoring of the wing [6]. The addition of a strut to alleviate bending moments allows for a smaller wing structure, with reduced wing thickness and chord length, thereby reducing transonic wave drag and spanwise crossflow disturbances [7]. For these reasons, recent studies in UHARW have focused on the Strut-Braced Wing (SBW) configuration for transonic mid-range aircraft [5,8,9]. Design studies for short- and long-range designs have also shown benefits over current designs [10].

Regarding propulsion, hydrogen-based concepts are active contenders for more sustainable aviation and the combination with SBWs to increase the overall benefits. As hydrogen does not emit CO<sub>2</sub>, the climate impact will be reduced compared to kerosene variants [11]. Hydrogen has a higher gravimetric energy density than kerosene, but a much lower volumetric energy density. Thus, while the total fuel mass is decreasing, the tanks required for storage necessitate a larger airframe. Cryogenic storage increases the density, but requires additional systems and insulation to keep temperatures low [12]. A selection of previous studies on conventional Liquid Hydrogen (LH<sub>2</sub>) aircraft designs, from short- to long-range aircraft, is presented in Table 1. The results show that hydrogen is a viable fuel for a wide variety of missions.

**Table 1.** Comparison of some existing conventional hydrogen-based aircraft concepts.

Category	Range	Passengers	OEM	MTOM	Fuel	Fuel Fraction	Reference
Regional	500 nm	72	14.6 t	22.9 t	0.8 t	3.5%	[13]
Short	1500 nm	180	48 t	68 t			[14]
Short	2160 nm	150	58.2 t	78 t	4.7 t	6.0%	[15]
Short	2462 nm	150	49.8 t	74.8 t	5.7 t	7.7%	[13]
Medium	2970 nm	180	57.1 t	79.3 t	6.3 t	7.9%	[16]
Medium	4000 nm	290	132 t	175 t			[14]
Medium	4860 nm	300	123 t	176 t	21 t	12.0%	[15]
Medium	4144 nm	295	136 t	205 t	24 t	11.7%	[13]
Long	5500 nm	420	149 t	224 t	24 t	10.7%	[17]
Long	7500 nm	380	113 t	184 t	31 t	16.7%	[18]
Long	10,260 nm	400	162 t	250 t	45 t	17.8%	[15]
Long	6400 nm	400	128 t	196 t	22 t	11.2%	[19]

UHARWs are intrinsically less rigid than conventional wings. This leads to geometrically non-linear behavior in deflections that cannot be accurately modeled using linear analysis models. These inaccuracies lead to errors in the conventional wing sizing models, as well as errors in wing weight estimation. As such, it is necessary to consider these geometric non-linearities due to the strut's deformation and apparent buckling under negative load cases [20]. Previous work has performed aerostructural optimization on kerosene-based SBWs [21,22]. The optimized wing showed a 30% reduction in wing weight and an 8% reduction in Maximum Take-Off Mass (MTOM) over the initial sizing using conventional handbook methods. Investigating the aerostructural effects on wing mass for SBWs becomes more important with a hydrogen-based concept, as the loss of fuel in the wings to act as bending moment relief has a large effect on the resulting wing stresses and hence requires higher wing structural mass. Previous studies indicate that the dry wing of LH<sub>2</sub> aircraft is typically expected to be 7–10% heavier than that of conventional kerosene-fueled aircraft [23]. This weight increase is primarily attributed to the absence of fuel within the wing structure, which in conventional designs helps to offload some of the structural loads during maneuvers with a positive load factor. Without the fuel's internal mass providing this offloading effect, the dry wing has to be structurally reinforced to handle the same loads, resulting in increased weight. Such findings align with the general

understanding that alternative fuel aircraft require significant structural modifications to maintain performance and safety standards.

This study compares the influence of LH2 propulsion on a medium-range SBW aircraft and evaluates the changes in aircraft design, operating costs, and emissions. Furthermore, aerostructural optimizations are performed for both wings to evaluate the impact of a dry wing on the wing mass for SBW aircraft and compare wing masses to a kerosene-based concept.

Section 2 describes the aircraft design framework as well as the models implemented to represent SBW aircraft and hydrogen networks. In Section 3, the resulting aircraft designs are compared by key performance parameters. Aerostructural optimizations of both wings are performed to evaluate the effects of a dry wing on the total mass. Finally, Section 4 provides conclusions of both investigations.

## 2. Methodology

The study investigates the influence of LH2 propulsion on a medium-range UHARW SBW aircraft. For the two concepts, LH2- and conventional kerosene-based, the basic aircraft design, operating costs, and emissions are compared. Furthermore, aerostructural optimizations are performed for the wing mass of SBW aircraft with and without wing fuel tanks under varying load constraints.

### 2.1. Conceptual Design

#### 2.1.1. Initial Sizing

The aircraft sizing and analysis procedure uses a two-step approach shown in Figure 1.

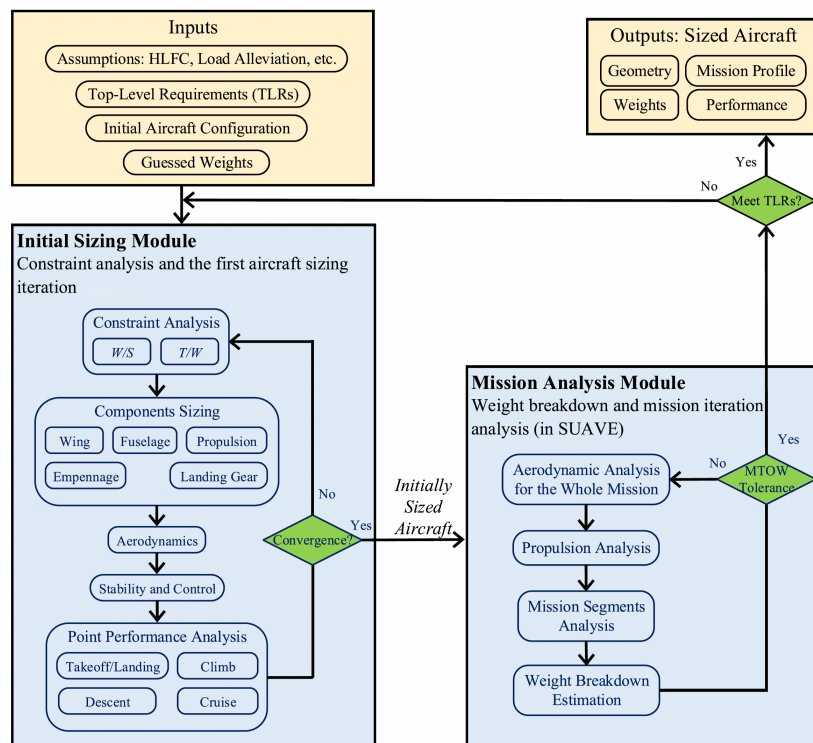


**Figure 1.** Conceptual aircraft sizing and analysis procedure.

The aircraft's initial sizing is performed using in-house conceptual sizing software [4,10], based on semi-empirical formulas and physics-based analysis methods. It is used to develop constraint diagrams for initial design point definition, as well as the fully defined and sized aircraft based on the chosen design point and top-level geometry definition parameters.

To create the constraint diagrams, a set of user-defined Top-Level Requirements (TLRs), including cruise altitude and airspeed, ground runs, ceilings, stall speeds, and climb rates, is required. Additionally, basic information regarding the desired aircraft configuration, such as wing planform parameters, average thickness, type of high-lift devices, and initial drag estimations, is needed. The constraint diagrams are then created using methods from Gudmundsson [24] and Loftin [25], while high-lift estimations are performed using Torenbeek [26] and Roskam [27]. The Oswald efficiency factor is estimated using the method presented by Nita [28], accounting for the given wing planform parameters. Following the design point determination, the wing, engines, and empennage are sized using methods from Torenbeek [26], Roskam [27], and Gudmundsson [24], updated for SBWs where necessary [10]. The resulting performance is cross-checked to ensure it remains within the performance given by the constraint diagram through simple aerodynamic and performance analyses. This process is iterated until a converged aircraft geometry results.

In a second step, the geometry is imported into the open-source Stanford University Aerospace Vehicle Environment (SUAVE) code [29]. The code contains modifications to include hydrogen-based power trains, hydrogen tank sizing and mass estimations [23,30], SBW, and UHARW geometry and weight estimations [10], as well as emission and cost analysis models [23,31], as described later in this section. SUAVE performs a full mission simulation and performance breakdown of the aircraft concept. It is used to fine-tune the aircraft concept for a consistent design capable of flying the design mission, including all relevant mission segments. It internally iterates for mass convergence and resizes the aircraft accordingly. With the mission-converged aircraft, a final check verifies that all initial TLRs and design requirements are still adhered to before delivering the final design. Otherwise, the sizing process will run again until all requirements are adhered to.

The main inputs to the mission analysis module are the aircraft geometry, initial MTOM estimation, and the flight mission specifications. The main mission is subdivided into three climb segments, a cruise segment, and five descent segments. The reserve mission is split into two climb segments, a diversion cruise, hold, and two descent segments. Within the vehicle setup, the engine is sized according to the Thrust-to-Weight Ratio (T/W) determined in the constraint diagram. For each mission segment, SUAVE uses a root-finding algorithm to find an equilibrium of forces, using angle of attack and thrust lever position as variables. The results are used to estimate the engine thrust and fuel flow along the mission segments. To determine the aircraft component masses, the FLOPS weight estimation method [32] is used. The combination of weight breakdown and total mission fuel is used to create a MTOM. This value is used as an iterable to determine if the aircraft concept has converged, or if the wing and propulsion system need to be resized according to the T/W and Wing Loading Ratio (W/S) values from the constraint diagram.

The basic SUAVE version does not include analysis modules for SBW concepts. For research into SBWs, a Class II wing weight estimation that includes mass terms for struts [33] is implemented in the mass module. This method is based on a physics-based wing weight estimation tool that takes aileron efficiency and aeroelastic effects into account.

A main advantage of the SBW configuration is that it enables higher aspect ratios than are currently common. These UHARW aircraft create some further design considerations that should be taken into account in the conceptual stage and are implemented in the presented sizing methodology. As LH2 will be stored in fuselage tanks, a correction factor to account for higher wing weight due to the dry wing of 7%, in line with current literature [23], is applied to the LH2 concept. Part of the presented study also investigates the validity of this assumption under different load cases in a later section.

One of these issues is compliance with airport gate restrictions. To adhere to International Civil Aviation Authority (ICAO) Class C gates and hence a wingspan of <36 m, the

wings need to be foldable, with an associated penalty in wing mass [34] included in the SBW weight estimation model as well.

To increase flow laminarity over the wing, the wing leading edge sweep angle should not exceed  $18^\circ$  to limit the transversal flow instabilities [35]. Regarding airfoils, the maximum thickness-to-chord ratio is chosen as 11.4% [8,35]. The wing thickness is kept constant from the wing root to the strut attachment position. The thickness-to-chord ratio is kept constant from the strut attachment to the wing folding position, and conventional thickness distributions are used for the remaining wing segment [8].

The strut is considered a structural element without any lift contribution to the aircraft at cruise. Structurally, it can be designed in a spindle shape since the chord is sized by buckling. The strut is attached to the main landing gear attachment in the fuselage and the main wing spar. It is designed with a symmetric airfoil of 18% maximum thickness-to-chord ratio [33].

### 2.1.2. Hydrogen Propulsion Network Model

The implemented hydrogen network model consists of corrections to the basic turbine performance cycle, fuel tank sizing, and mass estimations based on stresses [23,30]. The basic SUAVE engine model is implemented via a physics-based cycle analysis model [36]. Ultra High Bypass Ratio (UHBR) engines are used for the concept. Studies show that UHBR engines can reduce the Specific Fuel Consumption (SFC) by 21% compared to the conventional turbofan engines, such as the one currently modeled in SUAVE [37]. Furthermore, implementing the hydrogen expander cycle to convert the kerosene-burning engine models to hydrogen combustion reduces the SFC by another 4.3% [12]. Thus, a constant total SFC reduction of 25.3% is implemented while the engine diameter is increased by 30% [37] to account for both factors.

The mass estimations of the additional fuel system components due to the hydrogen network are split into two parts [23]. The fuel tank is actively sized through structural and thermodynamic analysis [38]. The peripherals are sized through constant terms [12].

The required fuel tank size is determined in an iterative manner by the required mission fuel, boil-off losses due to tank thermodynamics, and the fuselage geometry. This thermodynamic model estimates the internal pressure variations and tank heat transfer at each time step throughout the mission [39]. The heat transfer rate is a function of the insulation material and thickness. The total insulation is composed of several insulating layers, each acting as a thermal resistor in series with non-linear properties depending on its current temperature [38]. The total heat transfer rate resulting from this series of thermal resistors is implemented in the pressure equation [40] and solved iteratively for the unknown layer temperatures and heat transfer rate. Taking miscellaneous heat leaks due to other propulsion system components into account, the resulting boil-off is increased by 30%. Based on limit pressure constraints for fill and venting pressures, the liquid-to-tank fraction is computed [12,41]. The total tank volume and the required mission fuel mass are found in this fraction.

The resultant tank mass is found through an analysis of hoop and dome stresses of the resulting structure [38]. Using the limit load factor and the maximum pressure differential between the hydrogen and ambient conditions, the required structural wall thicknesses are computed, assuming aluminum as the tank material in this case.

### 2.1.3. Cost Estimation

The modified SUAVE includes an analysis of Direct Operating Costs (DOC) and production costs [23,31], based on [42]. DOC is used to compare the estimated market competitiveness of the two concepts. The total DOC is a summation of the energy, main-

tenance, capital, crew, and fee components [42]. A maintenance gain factor ( $k_g$ ) is added to Equation (1) to consider the influence of novel aircraft technology. This correction factor is assumed to account for the increased maintenance complexity of SBWs and the hydrogen network.

$$DOC = DOC_{Energy} + DOC_{Crew} + k_g DOC_{Maintenance} + DOC_{Capital} + DOC_{Fees} \quad (1)$$

The basic cost model for airframe pricing is based on Roskam [27], with the relevant correction factors for novel materials, unconventional aircraft, and design complexity set to the maximum value within Roskam's given ranges to model the expected development and manufacturing complexities of this unconventional design. A further addition to the capital cost was made to account for the LH2-tank cost [14]. The aircraft is assumed to fly 2000 cycles per year, in line with typical values for mid-range aircraft. For all labor costs and rates, 2010 values are used and inflation corrected for a comparison in 2050.

#### 2.1.4. Emission Estimation

A further point for comparison of the impact of a LH2 version on the SBW is equivalent emissions. The implemented emissions model [23,31] is based on methods shown in [11,43] to determine the Sustained Global Temperature Potential (SGTP).

For comparability, the final emissions are represented as equivalent CO<sub>2</sub>-emissions in Equation (2), accounting for actual CO<sub>2</sub>, NO<sub>x</sub>, contrails, cirrus clouds, and production emissions.

$$m_{CO_2,eq} = (k_0 EI_{CO_2} f_{km} + k_1 k_2 EI_{NO_x} f_{km} CF_{mid,NO_x} + k_3 k_4 CF_{mid,AIC}) \Delta R_{km} + m_{CO_2,eq,production} \quad (2)$$

The Emission Index (EI) for CO<sub>2</sub> is constant at 3.16; for NO<sub>x</sub>, it is dependent on fuel type and flight condition [44]. f<sub>km</sub> represents the fuel flow rate, and ΔR<sub>km</sub> represents the incremental flight range. The emissions for Aviation Induced Cloudiness (AIC), the combination of contrail and cirrus effects, are only a function of altitude and range in this model.

$$CF_{mid,NO_x} = \frac{SGTP_{O_{3s}}}{SGTP_{CO_2}} s_{O_{3s}} + \frac{SGTP_{O_{3L}}}{SGTP_{CO_2}} s_{O_{3L}} + \frac{SGTP_{CH_4}}{SGTP_{CO_2}} s_{CH_4} \quad (3)$$

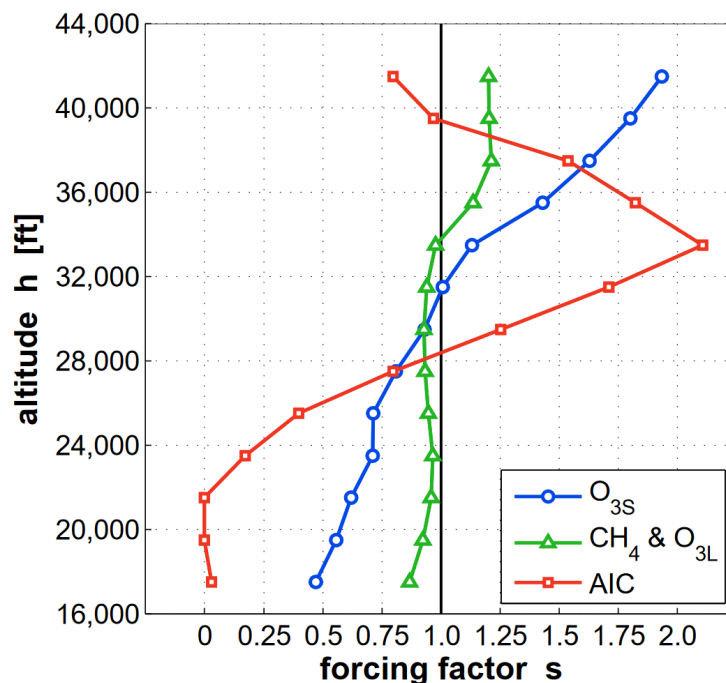
$$CF_{mid,AIC} = \frac{SGTP_{contrail}}{SGTP_{CO_2}} s_{contrail} + \frac{SGTP_{cirrus}}{SGTP_{CO_2}} s_{cirrus} + \frac{SGTP_{CH_4}}{SGTP_{CO_2}} s_{CH_4} \quad (4)$$

The correction factors for the emission species (CF) vary with aircraft altitude. To represent changes throughout the mission, the emission model is integrated into the SUAVE mission analysis to calculate local emissions along the mission. The CFs are defined in Equations (3) and (4). The values for SGTPs are taken from [45] and shown in Table 2. The forcing factors (s) as functions of altitude are obtained from [45] and shown in Figure 2.

Finally, the emissions are adapted to the fuel type in Equation (2) via constants k<sub>1</sub>–k<sub>4</sub>. Production effects are accounted for in the kerosene model as 22% of total flight emissions [31]. For the LH2 model, the emissions depend on the hydrogen production process. The model accounts for three types: green, blue, and gray hydrogen. The respective production emissions described in [46] are used in this model.

**Table 2.** SGTP indices for the emission species considered in the model [45].

Emittant	SGTP
CO <sub>2</sub>	$3.58 \times 10^{-14}$ [K/kg <sub>CO<sub>2</sub></sub> ]
O <sub>3s</sub>	$7.79 \times 10^{-12}$ [K/kg <sub>NO<sub>x</sub></sub> ]
O <sub>3L</sub>	$-9.14 \times 10^{-13}$ [K/kg <sub>NO<sub>x</sub></sub> ]
CH <sub>4</sub>	$-3.90 \times 10^{-12}$ [K/kg <sub>NO<sub>x</sub></sub> ]
Contrail	$1.37 \times 10^{-13}$ [K/km]
Cirrus	$4.12 \times 10^{-13}$ [K/km]

**Figure 2.** Radiative forcing factor data for NO<sub>x</sub> and AIC as function of altitude [45].

## 2.2. Coupled Adjoint Aerostructural Optimization

A coupled adjoint aerostructural wing optimization tool, FEMWET, was developed by Elham and van Tooren [47]. This tool seamlessly integrates a Quasi-Three-Dimensional (Q3D) aerodynamic solver with a finite beam element structural solver, utilizing the Newton method for tight coupling. Recently, Ma et al. [21] enhanced FEMWET by integrating a geometrically non-linear composite structural model, alongside modifying the Q3D solver to accommodate the analysis and optimization of Natural Laminar Flow (NLF).

FEMWET was originally developed as a versatile platform for conventional cantilevered wings. However, significant modifications were made to adapt it for UHARWs and, in particular, SBWs. These enhancements include the explicit modeling of the strut as a finite beam element and its coupling with the wing structure at the attachment points. Additionally, the structural model was refined to handle geometrically non-linear composite thin-walled beams. These advancements allow FEMWET to account for large displacements and rotations inherent to lightweight, flexible SBW designs. Further details on these modifications can be found in [21,48].

The integration of structural and aerodynamic solvers in FEMWET is managed through the Newton method, addressing the coupled problem of flexible UHARWs. The system is defined by four governing equations: those of the Vortex Lattice Method (VLM), Finite Element Method (FEM), level flight conditions, and the Q3D method. The tool uses finite beam elements placed at the wing box elastic axis to model the wing and strut structure. Both beams are connected at the wing/strut attachment point.

The aerostructural coupling includes a transfer of aerodynamic loads from the VLM mesh to the structural FEM mesh, and the transfer of displacements from the FEM to the VLM solver. This information transfer is performed through interpolation techniques. Figure 3 shows an example of the VLM and FEM meshes for the SBW.

In the optimization process, a gradient-based approach is employed, using a coupled adjoint derivative calculation for sensitivity analysis to enhance efficiency. FEMWET's novelty in this work lies in its first application to explore the influence of the dry wing concept on the wing structural weight for UHARWs. It is employed to investigate potential wing mass penalties due to the absence of fuel in the wings to act as a bending moment relief. The effects of different positive and negative initial load cases are investigated, as well as stiffness requirements for sufficient roll control due to aeroelastic effects.

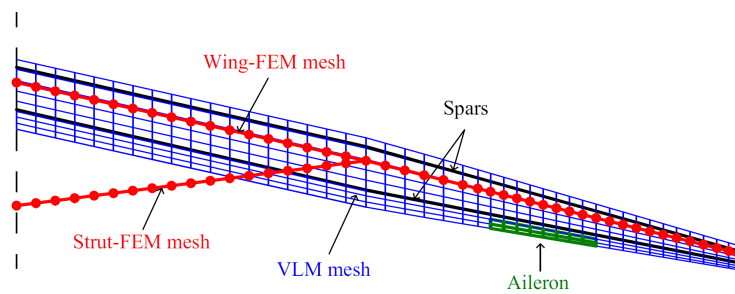


**Figure 3.** Example of aerodynamic and structural meshes for a SBW.

In the optimization process, a gradient-based approach is employed, using a coupled adjoint derivative calculation for sensitivity analysis to enhance efficiency.

In this study, FEMWET is used for an investigation of the influence of the dry wing concept on the wing structural weight for UHARWs. It is used to investigate potential wing mass penalties due to the absence of fuel in the wings to act as bending moment relief. The effects of different positive and negative limit load cases are investigated, as well as stiffness requirements for sufficient roll control due to aeroelastic effects.

### 3. Results

#### 3.1. Aircraft Conceptual Sizing

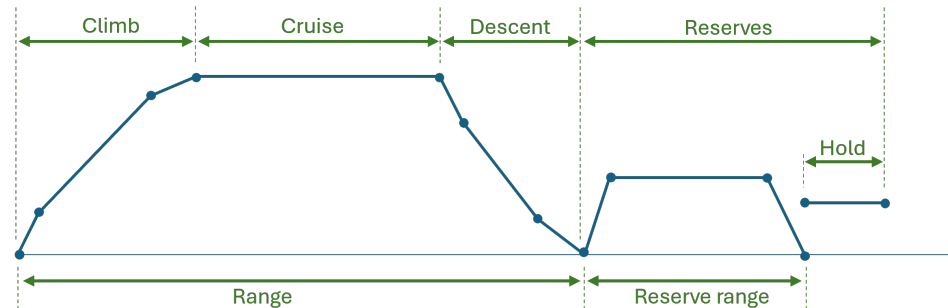
Both conventional and LH2-based aircraft are designed for EASA CS-25 requirements [49]. Initially, TLRs similar to the Airbus A320 have been considered. Ma et al. also performed a detailed sensitivity study to identify the most influential TLRs parameters and investigated their effect on aircraft performance, mainly to reduce energy consumption [50]. The outcome of that sensitivity study identified some changes in the TLRs to further improve aircraft energy efficiency, such as reducing the cruise Mach number to M0.735. The modified TLRs used to design the aircraft in this study are presented in Table 3.

The aircraft is designed with an aspect ratio of 25, based on other UHARW studies [8,51,52]. Due to the large resulting wingspan, the wing includes a folding mechanism to adhere to the 36 m wingspan requirement of an ICAO C-gate, similar to the A320. This feature is represented in the design through additional terms in the weight estimation module [34]. Furthermore, some advanced airframe technologies are considered for this next-generation passenger aircraft [10]: the strut-braced wing will use NLF airfoils. Hence, the percentage of laminar flow over the wing is increased to 50%, and 55% over the tail. Improvements in materials and structures, especially tow-steering of composites, allow a 20% weight reduction over metal structures. Improvements in control surface design and operation result in improved load alleviation opportunities. Hence, the maximum load factors can be reduced to +1.5 g and -0.5 g [53].

**Table 3.** Top-level design requirements for the SBW aircraft.

Parameter	Value
Cruise Mach number	0.735
Max. Mach number	0.82
Passengers	150
Range	3400 nm
Reserves	Contingency fuel Diversion range Holding (1500 ft)
Cruise altitude	33,000 ft
Service ceiling	38,500 ft
Takeoff field length	<6400 ft (ISA and sea level)
Landing distance	<4500 ft (ISA and sea level)
Approach speed	136 kts true airspeed
Airport (ICAO C)	Wing span Main landing gear span
Certification regulation	36 m 9 m CS-25

The aircraft's design mission profile is shown in Figure 4. Within the SUAVE framework, the mission is divided into multiple segments. The main mission range is 3400 nm, with a 200 nm diversion segment and 30 min of holding fuel. For the main mission, climb and descent are further discretized into three segments of constant speed and constant climb/descent rate. Furthermore, a reduced contingency factor of 3% of the trip fuel is applied [10].

**Figure 4.** SBW mission profile.

An earlier study has shown that fuel savings can be achieved for this aircraft configuration at a lower Mach number [50], hence the operating Mach was reduced from the baseline M0.78 to a more optimal M0.735 for the aircraft designs.

Figure 5 shows the resulting design points for the conventional kerosene-based and the LH<sub>2</sub>-based designs. Comparisons are made to the reference Airbus A320, as well as several other high aspect ratio wing concepts from literature: the SUGAR [8], SE2A-MR [4], D8.5 [52], and SD8.5 [2]. These concepts are all sized for a similar mission and passenger capacity and thus are suitable comparison points for the new design point. Within the sizing methodology, certain performance values regarding zero-lift drag of the airframe have to be assumed. These change depending on the final configuration. As such, the diagrams are updated in an iterative manner with the SUAVE mission simulation. The shown figures represent only the final converged performance values from the sizing process.

The Figure 5a shows that all SBWs have much lower T/W and W/S compared to the reference A320. All SBW design points, including the current design, are in the same region of the diagram, indicating that the difference to the A320 design point is inherent to the SBW design and to be expected. It also shows that stall speed/landing distance requirements

are not limiting this design and should thus open a large proportion of airports to potential service for the SBW designs. The current design is limited by the climb rate and service ceiling constraints, an expected result for a transport category aircraft. Figure 5b shows the changes in the constraints due to the conversion to LH<sub>2</sub> as a fuel type. As all other TLRs remain the same, the main change in the input parameters results from a higher zero-lift drag due to an extended fuselage housing the LH<sub>2</sub> tanks. Results show that while all flight-based constraints are moving towards higher T/W, the curved lines of the limiting constraints actually allow a small reduction in the required wing loading. Although cruise and turn constraints are more affected by the changes, they are still not limiting. The numerical design point values are shown in Table 4. It can be seen that the differences between the two concepts are small.

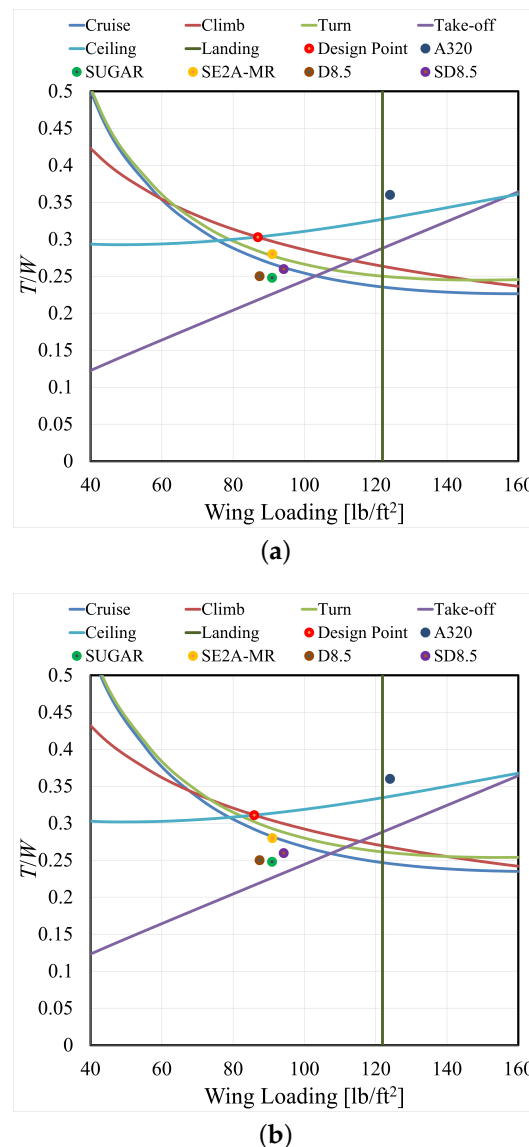


**Figure 5.** Constraint diagrams and selected design points for conventional SBW (a) and LH<sub>2</sub> SBW (b).

**Table 4.** Design points for both aircraft concepts.

	Kerosene	LH <sub>2</sub>
T/W [-]	0.3029	0.311
W/S [kg/m <sup>2</sup> ]	424.5	419.4

### 3.2. Geometries

The aircraft geometric definition is performed through the sizing procedure described in the previous section. The NASA supercritical airfoils SC(2)-0412 and SC(2)-0410 are used for the wing root and tip, respectively. The tail uses a NASA SC(2)-0010. The main wing quarter-chord sweep angle is set to 12.5 degrees, following a trade-off between flow laminarity and compressibility drag over the wing. The high-wing configuration features two UHBR turbofans between the wing and the struts, with a folding element outboard of the strut attachment. The chord of the strut is sized by buckling constraints, with an 18% thick airfoil for structural rigidity [54]. The key geometric parameters of both aircraft designs are summarized in Table 5.

**Table 5.** Aircraft geometry comparison between kerosene and LH2 SBW designs.

Parameter	Kerosene	LH2
Wing		
Aspect ratio	25	25
Span	63.65 m	64.66 m
Area	162.1 m <sup>2</sup>	167.2 m <sup>2</sup>
Taper ratio	0.35	0.35
Quarter chord sweep	12.5°	12.5°
Root chord	3.02 m	3.04 m
Dihedral	−1.5°	−1.5°
Root & kink thickness	12%	12%
Tip thickness	10%	10%
Strut		
Aspect ratio	23.03	23.03
Span	31.08 m	31.08 m
Area	41.97 m <sup>2</sup>	41.97 m <sup>2</sup>
Taper ratio	0.8	0.8
Quarter chord sweep	10°	10°
Root chord	1.5 m	1.5 m
Dihedral	11°	11°
Thickness	18%	18%
Vertical tail		
Aspect ratio	1	1
Span	5.7 m	5.17 m
Area	32.4 m <sup>2</sup>	26.8 m <sup>2</sup>
Taper ratio	1	1
Quarter chord sweep	40°	40°
Thickness	10%	10%
Horizontal tail		
Aspect ratio	5	5
Span	10.4 m	10.2 m
Area	21.7 m <sup>2</sup>	20.9 m <sup>2</sup>
Taper ratio	0.35	0.35
Quarter chord sweep	20°	20°
Dihedral	−3°	−3°
Thickness	10%	10%
Fuselage		
Length	39.0 m	52.4 m
Diameter	4.1 m	4.1 m

For visualization of the resulting concepts, Figure 6 showcases the resulting aircraft geometries, created in OpenVSP.

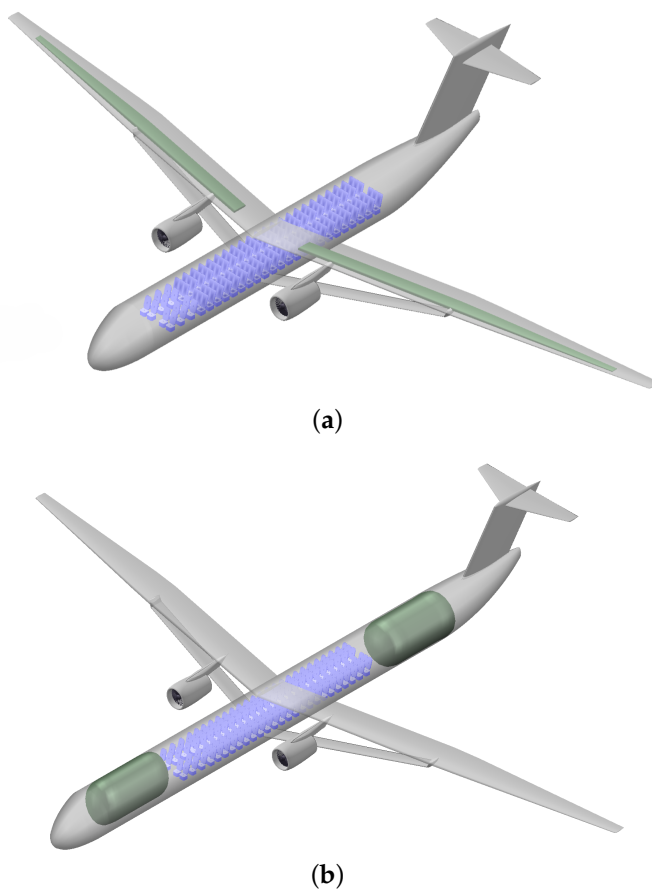


**Figure 6.** Isometric view of conventional (a) and LH2 (b) SBW aircraft concept.

A better comparison of the resulting geometries presented in Table 5, Figure 7 presents a top-view overlay of the two concepts, as well as the reference A320. The figure clearly shows the significantly larger, yet much more slender wing of the SBW designs. The folding element can be seen at an equivalent span location to the A320's winglets. It further shows that while the fuselage of the LH2 design is 13.4 m longer, the actual increase in wingspan and area is small. This is mostly due to structural mass differences being offset by fuel mass savings. Thus, no significant changes in wing design would be necessary to design LH2 SBW or conventional SBW aircraft.

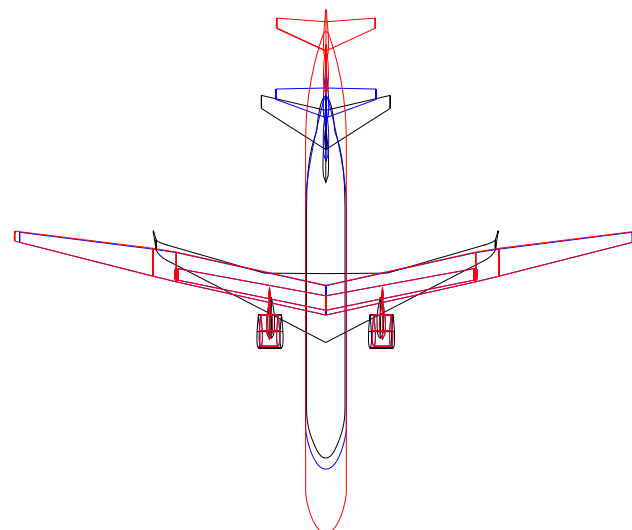


**Figure 7.** Aircraft design shape overlay of conventional (blue), LH2 (red), and A320 (black).

### 3.3. Masses

The resulting masses are shown in Table 6 and graphically in Figure 8. Table 6 shows the MTOM, fuel, and empty mass, including a component breakdown. The MTOM barely changes between the two designs. This is consistent with results from other studies [23] for conventional layouts. The higher gravimetric energy density of LH2 results in a reduction of 60% of the required mission fuel. This advantage is counteracted by the increase in fuselage size and hence mass, as well as the additional structural mass due to the LH2 tanks. The empty mass breakdown also shows a non-linear effect of the fuselage length on the mass. Despite only increasing by 13.4 m (34%) in length, the mass increases by 46.5%. An alleviating effect can be observed with the tail structure. Both the geometry and mass show reductions for the LH2 aircraft. The longer fuselage increases the moment arm of the tailplanes and hence allows for smaller surfaces for the same tail volume coefficient and stability/controllability requirements. The large wing mass increase of 10.7% is due to two factors. The generally larger design of the LH2 and hence the wing accounts for a 3.5% increase in mass. The further increase of 7% is due to larger structural requirements to account for a dry wing, and hence a reduction in wing bending moment relief [23]. Nevertheless, both aircraft show an 11–13% reduction in MTOM over the A320. The conventional SBW furthermore has 22% lower fuel and 14% lower empty mass. Thus, even the conventional SBW aircraft is already significantly lighter and more sustainable than current-generation aircraft.

**Table 6.** Aircraft mass comparison between kerosene and LH2 SBW designs.

Parameter	Conventional	LH2	Difference	A320 for Reference [55]
MTOM	68,802 kg	70,129 kg	+1.9%	79,000 kg
Fuel	16,381 kg	6543 kg	−60.0%	20,980 kg
Empty	38,201 kg	48,660 kg	+27.4%	44,300 kg
Propulsion	4696 kg	4906 kg	+4.5%	
Nacelles	536 kg	545 kg	+1.7%	
Landing gear	2319 kg	2360 kg	+1.8%	
Wing	9748 kg	10,791 kg	+10.7%	
Horizontal tail	415 kg	401 kg	−3.4%	
Vertical tail	905 kg	774 kg	−14.5%	
Fuselage	7066 kg	10,354 kg	+46.5%	
Systems	12,063 kg	12,569 kg	+4.2%	
LH2 tanks	−	6124 kg	−	
Paint	453 kg	542 kg	+19.6%	

The two pie charts in Figure 8 show how the relative breakdown changes between the two concepts. While the fuel mass accounts for nearly a quarter (23.8%) of the conventional MTOM, this reduces to about 10% for the LH2 design. The fuselage contribution increases from 10% to 15% MTOM, with the LH2 tanks taking up another 10%. As such, care should be taken in the conceptual design of LH2 aircraft if weight estimation methods are based on a specific fraction of the MTOM. For secondary parts such as landing gears, systems, or propulsion that are not affected much by this change, the differences are small. However, for all parts that are directly influenced by fuel volume or fuselage size, discretion is advised in the design phase.

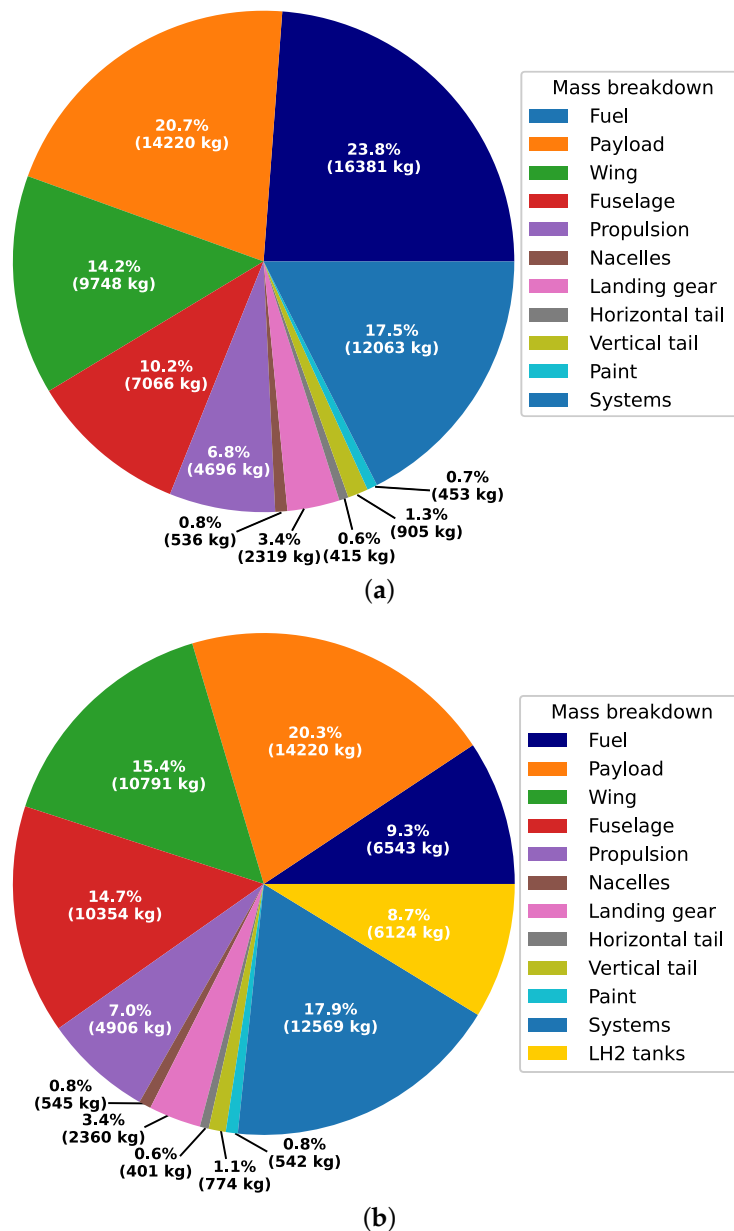


**Figure 8.** Mass breakdown for conventional SBW (a) and LH2 SBW (b).

### 3.4. Costs

Operating costs of the aircraft are shown in Figure 9 on a per flight and per seat-mile basis. The largest DOC component is the fuel. Despite the large difference in estimated unit fuel price (Jet-A 1.31 €/kg, LH2 3.04 €/kg), the LH2 fuel is 7% cheaper due to the lower required mission fuel mass. The largest discrepancy is seen in the maintenance costs. This is also the factor with the largest uncertainty. Due to the SBW configuration, a maintenance gain factor of 2 is assumed. The addition of a LH2 system is estimated with an additional factor of 1.5. Hence, for the LH2 aircraft, fuel and maintenance costs are expected to be approximately the same while for the conventional design, maintenance has a much smaller proportion. Capital costs are also expected to be higher, mostly due to the extra development costs of the cryogenic hydrogen systems and tanks. The propulsion type has only a negligible influence on the crew and fees. Thus, despite having lower overall fuel costs, the LH2 aircraft has 16% higher operating costs compared to the conventional kerosene version.

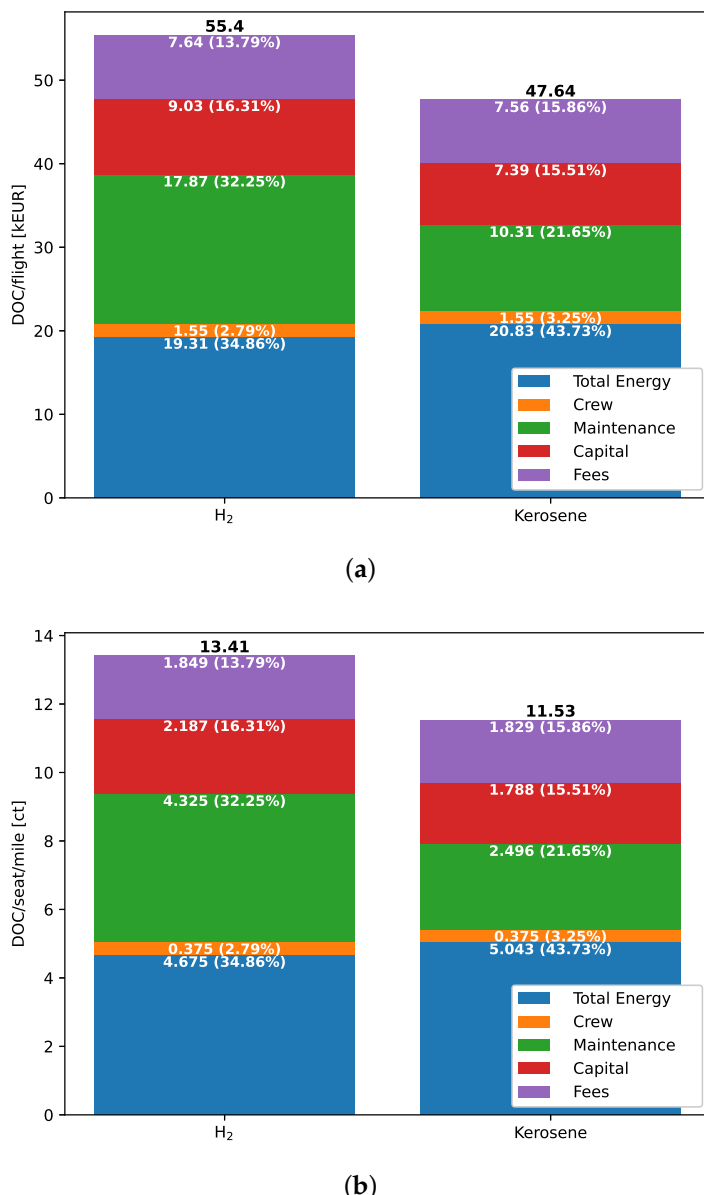


**Figure 9.** DOC breakdown for both aircraft designs on a per flight (a) and per seat-mile (b) basis.

### 3.5. Emissions

Emission results are compared in Figure 10. Although the actual emittants are different per phase, for comparability, all emissions are represented as CO<sub>2</sub> equivalents. For the LH<sub>2</sub> aircraft, the method of production has a major influence on the total emissions. For comparison, three different categories are shown. Grey hydrogen is created from natural gas or methane using the steam reforming process. Blue hydrogen is created through the same process, but the resulting CO<sub>2</sub> emissions are captured and stored. 10–20% of the generated carbon cannot be captured; thus, this is a ‘low-emission’ generation. Green hydrogen is the only ‘clean’ hydrogen generation, produced by splitting water using electricity generated by renewable sources. The results show that the production emissions for blue hydrogen are ~10% lower than for grey hydrogen. Despite the majority of carbon created in the gas-burning process being captured, the additional energy required to drive the capture and storage process negates most of this benefit. The additional complexity of the production process also results in higher production emissions than kerosene. Green hydrogen has no production emissions due to the water hydrolysis process.

Hydrogen has a higher flame temperature and would thus create higher  $\text{NO}_x$  emissions at a similar equivalence ratio. However, the wider flammability limits of hydrogen allow for leaner combustion and thus a lower resultant flame temperature, which can significantly reduce the overall  $\text{NO}_x$  emissions to ~35% of kerosene. The AIC results from contrails and cirrus clouds due to emitted water freezing. Hydrogen has 2.58 times higher water emissions. However, due to much lower soot levels in the exhaust, the created ice crystals are larger and optically thinner. These effects are opposite but approximately equal in magnitude, leading to a 7% reduction in overall AIC for the hydrogen aircraft. Overall emission levels are 57–82% of the kerosene aircraft, depending on the LH2 source. Results show the relevance of green sources for LH2 production for more sustainable aviation, but also that even then, hydrogen-powered aviation is far from climate-neutral.

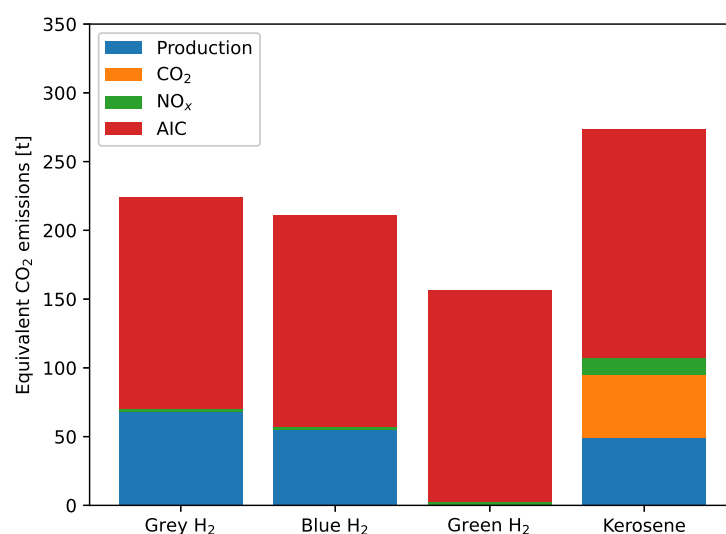


**Figure 10.** Production and in-flight emissions for the aircraft concepts, converted to equivalent  $\text{CO}_2$  emissions.

### 3.6. Wing Structure Optimization Results

This section describes a series of wing aeroelastic optimizations using the FEMWET tool to investigate the structural design and weight of dry and wet wings of the created SBW concepts and evaluate potential weight penalties due to the absence of fuel in the wing to act as bending moment relief. FEMWET calculates the inertial loads due to the wing and fuel masses for aeroelastic analysis and structural optimization. The difference between the dry and wet wings can be considered by removing the fuel from the wing. The consequences are automatically considered in the FEMWET simulation.

The MTOM of the LH2 aircraft is approximately 2% larger compared to the kerosene aircraft, as given in Table 7. However, despite the higher MTOM, the wing loading is approximately 3% lower for the LH2 design. This reduction in wing loading is attributed to the additional drag of the longer fuselage, which requires a lower wing loading to maintain the same takeoff and landing requirements.

**Table 7.** Key parameter comparison between kerosene and LH2 SBW designs.

Configuration	MTOM	$S_w$	Fuel Mass
Conventional	68,802 kg	159.9 $\text{m}^2$	16,381 kg
LH2	70,129 kg	167.9 $\text{m}^2$	6543 kg
Difference	+1.93%	+5.0%	-60.0%

To investigate the dry wing behavior, a series of aeroelastic optimizations are performed for both the dry and the wet wings of the LH2 and conventional aircraft designed in this research. The optimization formulation is presented as follows:

$$\begin{aligned}
 & \text{minimize} && W_{w+s}(X) \\
 & \text{with regard to} && x = [t_{u,i}, t_{s,i}, t_{fs,i}, t_{rs,i}] \\
 & \text{subject to} && \begin{cases} \text{Failure}_k \leq 0 \\ 1 - \frac{L_s}{L_{s,\min}} \leq 0 \\ X_{\text{lower}} \leq X \leq X_{\text{upper}} \end{cases} \quad (5)
 \end{aligned}$$

The wing and strut are segmented along the span into 15 and 7 sections, respectively, each comprising four equivalent panels: the upper skin (including stringers), lower skin (including stringers), front spar, and rear spar. The thicknesses of these panels are defined as design variables. Therefore, a total of 88 design variables are utilized. Each equivalent panel is subdivided into four elements for stress and failure criteria calculations, while each spar panel is divided into two elements for the same purpose. The failure criteria encompass tension and compression failures, as well as Euler and shear buckling. Overall, the optimization includes 3072 constraints on structural failure and one constraint on aileron effectiveness. Previous research has shown that aileron effectiveness is an active constraint in deriving the structural design of the wing [21]. The structural weight of the wing has been shown to increase quadratically with the requirements for the effectiveness of the aileron [56]. Therefore, such a constraint is added to ensure the roll performance requirement of the aircraft can be satisfied. In this constraint,  $L_s$  and  $L_{s,\min}$  represent the derivative of the roll moment due to aileron deflection for the wing and the minimum required value to meet the roll requirements, respectively. More detail on the aileron design for this SBW and the importance of including roll moments in an aerostructural optimization for SBWs can be found in [56].

The primary objective of this research is to investigate the differences in structural design and mass between wet and dry wings. To investigate how the presence or absence of fuel within the wing affects the overall design and performance of the wing structure under various load conditions, multiple optimizations are performed to design the wing structures for both conventional (wet) and LH2 (dry) configurations. These optimizations involve the minimization of the wing mass under different load cases, including positive and negative g-loads, as well as roll maneuvers. The roll moment requirements in this study are derived from flying quality regulations such as MIL-F-8785C for the transport aircraft class [57]. The aileron layout and sizing are described in detail in [56].

Table 8 provides an overview of the different load cases considered for aeroelastic optimizations of the SBW aircraft. These include pull-up and push-down maneuvers, roll conditions, and cruise scenarios, each characterized by different weight, altitude, Mach number, and load factors. Flight altitude and speed are based on an analysis of critical load cases within the flight envelope of the aircraft, similar to [58]. These do not necessarily correspond to operational limitations, but ensure structural integrity at all critical points within the designated flight envelope. The reduced load factors of 1.5 and  $-0.5$  (instead of 2.5 and  $-1$ ) are based on the assumption of a load alleviation technology [21].

By analyzing these variations, the aim is to gain insights into the structural reinforcements necessary for dry wings, which lack the internal fuel mass that typically aids in load distribution in wet wings. This comprehensive analysis helps in understanding the impact of fuel presence on the wing's structural integrity and informs the design considerations for future alternative fuel aircraft.

**Table 8.** Load cases of the SBW aircraft.

Load Case	Type	Weight	Altitude [m]	Mach	Load Condition [g]
1	Pull-up	$W_{TO}$	7500	0.78	1.5
2	Push-down	$W_{TO}$	7500	0.78	-0.5
3	Roll	$W_{des}$	4000	0.75	1
4	Cruise	$W_{des}$	10,058	0.735	1

Table 9 provides the aeroelastic optimization results of the wing for single load conditions, presented as resulting masses for the wing ( $m_w$ ), strut ( $m_{st}$ ), and total wing system ( $m_{w+st}$ ). Under the +1.5 g load condition, the LH2 design is 13.8% heavier than the conventional design. In the +2.5 g load condition, the LH2 wing is significantly heavier by 16.8%. The increased weight is attributed to the structural reinforcements required to handle the higher loads in wing structures. For the -0.5 g load condition, the LH2 wing is only 4.2% heavier than the conventional wing. This difference is smaller because the negative load case does not benefit from the fuel's weight reduction compared to positive load cases. Here, the fuel weight in the wing increases the loads on the wing rather than decreasing them, making the wet wing almost as heavy as the dry wing, despite its lower MTOM. Under the -1.0 g load condition, the LH2 design shows a 7.7% increase in weight. Under this condition, wing-based fuel does not provide any bending moment relief for either concept. The higher MTOM of the LH2 aircraft leads to higher structural loads which, together with the larger wing area, result in a heavier wing structure.

**Table 9.** Aeroelastic wing mass optimization results for single load conditions.

Configuration	Load Condition	$m_{w+st}$ , kg	$m_w$ , kg	$m_{st}$ , kg
Conventional	+1.5 g	7300	5685	1616
LH2	+1.5 g	8473	6747	1726
Difference		+13.8%	+15.7%	+6.37%
Conventional	+2.5 g	8040	6361	1679
LH2	+2.5 g	9669	7883	1786
Difference		+16.8%	+19.3%	+5.99%
Conventional	-0.5 g	7467	5818	1646
LH2	-0.5 g	7792	6103	1686
Difference		+4.21%	+4.67%	+2.37%
Conventional	-1.0 g	8702	6983	1719
LH2	-1.0 g	9425	7650	1775
Difference		+7.67%	+8.71%	+3.15%

After this insight, a new series of optimizations has been performed to investigate a more realistic wing structural design, including both positive and negative static loads as well as roll moment requirements. Previous studies on wing aerostructural design optimization have shown that the requirements for roll performance, i.e., the influence of aeroelastic effects on aileron effectiveness, can have a large influence on wing structural design and mass [21,59]. Table 10 presents the full optimization results for various load conditions. A notable outcome is that the wing weight is the same under 1.5 g/-0.5 g and 2.5 g/-1 g. This indicates that, indeed, the aileron effectiveness constraint was the critical condition for wing structural design and mass, in line with the previous studies [21,56]. Under the +1.5 g/-0.5 g load condition with a roll moment constraint, the LH2 design is only 1.75% heavier. The weight increase under multi-load conditions is primarily driven by the necessity to balance both positive and negative load cases, with the latter having a dominant effect. For the +2.5 g/-1.0 g load condition with a roll moment constraint, the

same masses can be observed. Thus, for this SBW design, the aileron effectiveness and roll moment constraint supersedes the maximum load case requirements for both conventional and LH2 versions. The heavier structure is necessary to meet the higher load requirements imposed by the roll moment constraint.

**Table 10.** Aeroelastic wing mass optimization results for combined load cases incl. roll requirements.

Configuration	Load Condition	$m_{w+s}$ , kg	$m_w$ , kg	$m_{st}$ , kg
Conventional	+1.5 g / −0.5 g/Roll	14,117	12,123	1994
LH2	+1.5 g / −0.5 g/Roll	14,368	12,359	2009
Difference		+1.75%	+1.91%	+0.747%
Conventional	+2.5 g / −1.0 g/Roll	14,117	12,123	1994
LH2	+2.5 g / −1.0 g/Roll	14,368	12,359	2009
Difference		+1.75%	+1.91%	+0.747%

From the optimization results in Table 9, it can be seen that the structural weight penalty of the wing structure from the dry wing design strongly depends on the applied load case. For a final design using +2.5 g / −1 g as design load factors, the difference in wing mass can be up to 17%. This is significantly higher than other studies investigating SBW aircraft, which estimate that the dry wing of LH2 aircraft is typically expected to be 7–10% heavier than that of conventional kerosene-fueled aircraft [23].

On the other hand, when including roll rate requirements in the wing design and optimization, as shown in Table 10, it can be seen that the structural weight penalty of the wing structure from the dry wing design is not large for this SBW aircraft under study. However, the total mass of the wing has increased by 48.6% (LH2) and 75.6% (conventional). As such, the importance of aileron design and placement significantly outweighs the effects of wet or dry wings for UHARW and SBW aircraft and needs to be taken into account already at a conceptual design level for credible results.

#### 4. Conclusions

The study investigates the influence of Liquid Hydrogen (LH2) propulsion on a medium-range Strut-Braced Wing (SBW) aircraft by comparing the LH2 to a kerosene-based SBW aircraft designed with the same top-level requirements. For the two aircraft, overall design, operating costs, and emissions are compared. Furthermore, aerostructural optimizations are performed for the wing mass of SBW aircraft with and without wing fuel tanks.

Initial sizing is performed using a highly modified version of the open-source Stanford University Aerospace Vehicle Environment (SUAVE) tool, with modules to estimate the performance of hydrogen direct burn engines and hydrogen tank sizing, correlations for Ultra-High Aspect Ratio Wing (UHARW) weight estimations, as well as Direct Operating Costs (DOC) and emission estimations.

For the same set of Top-Level Requirements (TLRs), the results show that the main difference in the design point definition results from a higher zero-lift drag due to an extended fuselage housing the LH2 tanks, with a small reduction in the required wing loading. The increase in total wingspan and area is small because the structural mass increases of the LH2 aircraft due to additional tanks and fuselage structure are offset by fuel mass savings. Both aircraft show an 11–13% reduction in Maximum Take-Off Mass (MTOM) over the A320. The conventional SBW furthermore has 22% lower fuel requirement and a 14% lower empty mass. Both SBWs have much lower Thrust-to-Weight Ratio (T/W) and Wing Loading Ratio (W/S) compared to reference A320. While the fuel mass accounts for nearly a quarter (23.8%) of the kerosene design's MTOM, this reduces to about 10% for the

LH2 design. The fuselage contribution increases from 10% to 15% MTOM, with the LH2 tanks taking up another 10%.

For the LH2 aircraft, overall fuel costs are expected to be approximately equal to those of the conventional design. Capital and maintenance costs are expected to be higher, mostly due to the extra development costs and maintenance complexity of the cryogenic hydrogen systems and tanks. Overall, the LH2 aircraft has 16% higher operating costs compared to the conventional kerosene version. On the other side, overall emission levels are 57–82% of the kerosene aircraft, depending on the LH2 production method, and there is a 7% reduction in overall contrail emissions for the LH2 aircraft.

It is hence concluded that no significant changes in wing design would be necessary to design LH2 SBWs compared to conventional SBW aircraft. While the fuel mass reduces for the LH2 design, the extended fuselage housing the LH2 tanks contributes to an increase in weight. Thus, care should be taken in the conceptual design of LH2 aircraft if weight estimation methods are based on a specific fraction of the MTOM. Even the conventional SBW aircraft is already significantly lighter and more sustainable than current generation aircraft.

For static loads, the absence of fuel acting as bending moment relief in the wing results in a 17% increase in wing structural mass. However, if roll rate constraints are included in the wing design process, then much more restrictive aileron effectiveness requirements cause a large increase in overall wing weight for both aircraft, with the difference due to a dry wing reducing to less than 2%. As such, the importance of aileron design and placement significantly outweighs the effects of wet or dry wings for UHARW and SBW aircraft, and needs to be taken into account already at a conceptual design level for credible results.

**Author Contributions:** Conceptualization, N.F.M.W. and A.E.; methodology, N.F.M.W., Y.M. and A.E.; software, N.F.M.W. and A.E.; validation, N.F.M.W. and A.E.; writing—original draft preparation, N.F.M.W. and Y.M.; writing—review and editing, N.F.M.W. and A.E.; visualization, N.F.M.W.; supervision, A.E.; project administration, A.E.; funding acquisition, A.E. All authors have read and agreed to the published version of the manuscript.

**Funding:** This work was supported by the Natural Environment Research Council [NE/Z503824/1].

**Data Availability Statement:** The original contributions presented in this study are included in the article. Further inquiries can be directed to the corresponding author.

**Conflicts of Interest:** Author Yiyuan Ma was employed by the company Bauhaus Luftfahrt e.V. The remaining authors declare that the research was conducted in the absence of any commercial or financial relationships that could be construed as a potential conflict of interest.

## Abbreviations

AIC	Aviation Induced Cloudiness
DOC	Direct Operating Costs
EI	Emission Index
FEM	Finite Element Method
ICAO	International Civil Aviation Authority
LH2	Liquid Hydrogen
MTOM	Maximum Take-Off Mass
NLF	Natural Laminar Flow
Q3D	Quasi-Three-Dimensional
SBW	Strut-Braced Wing
SFC	Specific Fuel Consumption

SGTP	Sustained Global Temperature Potential
SUAVE	Stanford University Aerospace Vehicle Environment
T/W	Thrust-to-Weight Ratio
TLR	Top-Level Requirement
UHARW	Ultra-High Aspect Ratio Wing
UHBR	Ultra High Bypass Ratio
VLM	Vortex Lattice Method
W/S	Wing Loading Ratio

## References

1. Advisory Council for Aviation Research and Innovation in Europe. *Realising Europe's Vision for Aviation, Strategic Research & Innovation Agenda*; Technical Report; ACARE: Brussels, Belgium 2012.
2. Greitzer, E.M.; Bonnefoy, P.; De la Rosa Blanco, E.; Dorbian, C.; Drela, M.; Hall, D.; Hansman, R.; Hileman, J.; Liebeck, R.; Lovegren, J.; et al. *N+3 Aircraft Concept Designs and Trade Studies, Final Report*; NASA/CR-2010-216794/VOL1; NASA Glenn Research Center: Cleveland, OH, USA, 2010.
3. Ma, Y.; Elham, A. Designing high aspect ratio wings: A review of concepts and approaches. *Prog. Aerosp. Sci.* **2024**, *145*, 100983. [\[CrossRef\]](#)
4. Karpuk, S.; Elham, A. Conceptual design trade study for an energy-efficient mid-range aircraft with novel technologies. In Proceedings of the AIAA Scitech 2021 Forum, Virtual, 11–15 & 19–21 January 2021; p. 0013.
5. Hosseini, S.; Ali Vaziri-Zanjani, M.; Reza Ovesy, H. Conceptual design and analysis of an affordable truss-braced wing regional jet aircraft. *Proc. Inst. Mech. Eng. Part G. Aerosp. Eng.* **2020**, *0954410020923060*. [\[CrossRef\]](#)
6. Gur, O.; Schetz, J.A.; Mason, W.H. Aerodynamic considerations in the design of truss-braced-wing aircraft. *J. Aircr.* **2011**, *48*, 919–939. [\[CrossRef\]](#)
7. Shirley, C.M.; Schetz, J.A.; Kapania, R.K.; Haftka, R.T. Tradeoffs of wing weight and lift/drag in design of medium-range transport aircraft. *J. Aircr.* **2014**, *51*, 904–912. [\[CrossRef\]](#)
8. Bradley, M.K.; Droney, C.K. *Subsonic Ultra Green Aircraft Research: Phase II—Volume II—Hybrid Electric Design Exploration*; NASA/CR-2015-218704/VOL2; NASA Langley Research Center: Hampton, VA, USA, 2015.
9. Torrigiani, F.; Bussemaker, J.; Ciampa, P.D.; Fioriti, M.; Tomasella, F.; Aigner, B.; Rajpal, D.; Timmermans, H.; Savelyev, A.; Charbonnier, D.; et al. *Design of the Strut Braced Wing Aircraft in the AGILE Collaborative MDO Framework*; In Proceedings of the 31st Congress of the International Council of the Aeronautical Sciences, ICAS, Belo Horizonte, Brasil, 9–14 September 2018.
10. Ma, Y.; Karpuk, S.; Elham, A. Conceptual design and comparative study of strut-braced wing and twin-fuselage aircraft configurations with ultra-high aspect ratio wings. *Aerosp. Sci. Technol.* **2022**, *121*, 107395. [\[CrossRef\]](#)
11. Scholz, D. Calculation of the Emission Characteristics of Aircraft Kerosene and Hydrogen Propulsion. Harvard Data-Verse. 2020. Available online: <https://dataVERSE.harvard.edu/dataset.xhtml?persistentId=> (accessed on 20 May 2024). [\[CrossRef\]](#)
12. Brewer, G.D. *Hydrogen Aircraft Technology*; CRC Press: Boca Raton, FL, USA, 1991.
13. Onorato, G.; Proesmans, P.; Hoogreef, M. Assessment of hydrogen transport aircraft: Effects of fuel tank integration. *CEAS Aeronaut. J.* **2022**, *13*, 813–845. [\[CrossRef\]](#) [\[PubMed\]](#)
14. Hoelzen, J.; Silberhorn, D.; Zill, T.; Bensmann, B.; Hanke-Rauschenbach, R. Hydrogen-powered aviation and its reliance on green hydrogen infrastructure—Review and research gaps. *Int. J. Hydrogen Energy* **2022**, *47*, 3108–3130. [\[CrossRef\]](#)
15. Verstraete, D. On the energy efficiency of hydrogen-fuelled transport aircraft. *Int. J. Hydrogen Energy* **2015**, *40*, 7388–7394. [\[CrossRef\]](#)
16. White, A.S.; Waddington, E.; Greitzer, E.M.; Merret, J.M.; Ansell, P.J.; Hall, D.K. Trade-space assessment of liquid hydrogen propulsion systems for electrified aircraft. In Proceedings of the AIAA Aviation 2023 Forum, San Diego, CA, USA, 12–16 June 2023; p. 4345.
17. Adler, E.J.; Martins, J.R. Blended wing body configuration for hydrogen-powered aviation. *J. Aircr.* **2024**, *61*, 887–901. [\[CrossRef\]](#)
18. Verstraete, D. Long range transport aircraft using hydrogen fuel. *Int. J. Hydrogen Energy* **2013**, *38*, 14824–14831. [\[CrossRef\]](#)
19. Troeltsch, F.M.; Engelmann, M.; Scholz, A.E.; Peter, F.; Kaiser, J.; Hornung, M. Hydrogen powered long haul aircraft with minimized climate impact. In Proceedings of the AIAA Aviation 2020 Forum, Online, 15–19 June 2020; p. 2660.
20. Sohst, M.; do Vale, J.L.; Afonso, F.; Suleman, A. Optimization and comparison of strut-braced and high aspect ratio wing aircraft configurations including flutter analysis with geometric non-linearities. *Aerosp. Sci. Technol.* **2022**, *124*, 107531. [\[CrossRef\]](#)
21. Ma, Y.; Abouhamzeh, M.; Elham, A. Geometrically nonlinear coupled adjoint aerostructural optimization of natural-laminar-flow strut-braced wing. *J. Aircr.* **2023**, *60*, 935–954. [\[CrossRef\]](#)
22. Ma, Y.; Abouhamzeh, M.; Elham, A. Aerostructural optimization and comparative study of twin-fuselage and strut-braced-wing aircraft configurations. *J. Aircr.* **2024**, *61*, 839–856. [\[CrossRef\]](#)

23. Karpuk, S.; Elham, A. Comparative study of hydrogen and kerosene commercial aircraft with advanced airframe and propulsion technologies for more sustainable aviation. *Proc. Inst. Mech. Eng. Part G J. Aerosp. Eng.* **2023**, *237*, 2074–2091. [[CrossRef](#)]

24. Gudmundsson, S. *General Aviation Aircraft Design: Applied Methods and Procedures*; Butterworth-Heinemann: Oxford, UK, 2013.

25. Loftin, L.K., Jr. *Subsonic Aircraft: Evolution and the Matching of Size to Performance*; NASA-RP-1060; NASA Langley Research Center: Hampton, VA, USA, 1980.

26. Torenbeek, E. *Synthesis of Subsonic Airplane Design*; Delft University Press: Delft, The Netherlands, 1982.

27. Roskam, J. *Airplane Design Part I–VIII*; Roskam Aviation and Engineering Corp.: Ottawa, KS, USA, 1985.

28. Niță, M.; Scholz, D. Estimating the Oswald factor from basic aircraft geometrical parameters. In Proceedings of the Deutscher Luft- und Raumfahrtkongress 2012, Berlin, Germany, 10–12 September 2012.

29. Lukaczyk, T.W.; Wendorff, A.D.; Colonna, M.; Economou, T.D.; Alonso, J.J.; Orra, T.H.; Ilario, C. SUAVE: An open-source environment for multi-fidelity conceptual vehicle design. In Proceedings of the 16th AIAA/ISSMO Multidisciplinary Analysis and Optimization Conference, Dallas, TX, USA, 22–26 June 2015; p. 3087.

30. Karpuk, S.; Ma, Y.; Elham, A. Design Investigation of Potential Long-Range Hydrogen Combustion Blended Wing Body Aircraft with Future Technologies. *Aerospace* **2023**, *10*, 566. [[CrossRef](#)]

31. Karpuk, S.; Radespiel, R.; Elham, A. Assessment of future airframe and propulsion technologies on sustainability of next-generation mid-range aircraft. *Aerospace* **2022**, *9*, 279. [[CrossRef](#)]

32. Wells, D.P.; Horvath, B.L.; McCullers, L.A. *The Flight Optimization System Weights Estimation Method*; Technical Report NASA/TM-2017-219627/VOL1; NASA Langley Research Center: Hampton, VA, USA, 2017.

33. Chiozzotto, G.P. Initial weight estimate of advanced transport aircraft concepts considering aeroelastic effects. In Proceedings of the 55th AIAA Aerospace Sciences Meeting, Grapevine, TX, USA, 9–13 January 2017; p. 0009.

34. Gur, O.; Bhatia, M.; Mason, W.H.; Schetz, J.A.; Kapania, R.K.; Nam, T. Development of a framework for truss-braced wing conceptual MDO. *Struct. Multidiscip. Optim.* **2011**, *44*, 277–298. [[CrossRef](#)]

35. Carrier, G.; Atinault, O.; Dequand, S.; Hantrais-Gervois, J.L.; Liauzun, C.; Paluch, B.; Rodde, A.M.; Toussaint, C. Investigation of a strut-braced wing configuration for future commercial transport. In Proceedings of the 28th Congress of the International Council of the Aeronautical Sciences, ICAS, Brisbane, Australia, 23–28 September 2012.

36. Merkl, E. *Final Report Summary-ENOVAL (Engine Module Validators)*; European Commission: Amsterdam, The Netherlands, 2018.

37. Giesecke, D.; Lehmler, M.; Friedrichs, J.; Blinstrub, J.; Bertsch, L.; Heinze, W. Evaluation of ultra-high bypass ratio engines for an over-wing aircraft configuration. *J. Glob. Power Propuls. Soc.* **2018**, *2*, 493–515. [[CrossRef](#)]

38. Verstraete, D. The Potential of Liquid Hydrogen for Long Range Aircraft Propulsion. Ph.D. Thesis, Cranfield University, Cranfield, UK, 2009.

39. Lin, C.S.; Van Dresar, N.T.; Hasan, M.M. Pressure control analysis of cryogenic storage systems. *J. Propuls. Power* **2004**, *20*, 480–485. [[CrossRef](#)]

40. Winnefeld, C.; Kadyk, T.; Bensmann, B.; Krewer, U.; Hanke-Rauschenbach, R. Modelling and designing cryogenic hydrogen tanks for future aircraft applications. *Energies* **2018**, *11*, 105. [[CrossRef](#)]

41. Verstraete, D.; Hendrick, P.; Pilidis, P.; Ramsden, K. Hydrogen fuel tanks for subsonic transport aircraft. *Int. J. Hydrogen Energy* **2010**, *35*, 11085–11098. [[CrossRef](#)]

42. Bardenhagen, A.; Gobbin, A. *Flugzeugentwurf II*; Universität Stuttgart: Stuttgart, Germany, 2017.

43. Scholz, D. Design of hydrogen passenger aircraft: How much “zero-emission” is possible? In Proceedings of the Hamburg Aerospace Lecture Series (DGLR, RAeS, VDI, ZAL, HAW Hamburg), Online, 19 November 2020.

44. Baughcum, S.L.; Tritz, T.G.; Henderson, S.C.; Pickett, D.C. *Scheduled Civil Aircraft Emission Inventories for 1992: Database Development and Analysis*; Technical Report NASA-CR-4700; NASA Langley Research Center: Hampton, VA, USA, 1996.

45. Dallara, E.S. Aircraft Design for Reduced Climate Impact. Ph.D. Thesis, Stanford University, Stanford, CA, USA, 2011.

46. Howarth, R.W.; Jacobson, M.Z. How green is blue hydrogen? *Energy Sci. Eng.* **2021**, *9*, 1676–1687. [[CrossRef](#)]

47. Elham, A.; van Tooren, M.J. Coupled adjoint aerostructural wing optimization using quasi-three-dimensional aerodynamic analysis. *Struct. Multidiscip. Optim.* **2016**, *54*, 889–906. [[CrossRef](#)]

48. Abouhamzeh, M.; Ma, Y.; Elham, A. A Geometrically Nonlinear Structural Model For Aerostructural Optimization of Ultra-High Aspect Ratio Composite Wings. In Proceedings of the AIAA SciTech 2022 Forum, San Diego, CA, USA, 3–7 January 2022; p. 0724.

49. EASA. *CS-25 Large Aeroplanes, Amendment 28*; Technical Report; European Union Aviation Safety Agency: Cologne, Germany, 2023.

50. Ma, Y.; Minisci, E.; Elham, A. Investigating the influence of uncertainty in novel airframe technologies on realizing ultra-high aspect ratio wings. In Proceedings of the AeroBest 2021, Lisboa, Portugal, 21–23 July 2021.

51. Brooks, T.R.; Martins, J.R.; Kennedy, G.J. High-fidelity aerostructural optimization of tow-steered composite wings. *J. Fluids Struct.* **2019**, *88*, 122–147. [[CrossRef](#)]

52. Yutko, B.M.; Titchener, N.; Courtin, C.; Lieu, M.; Wirsing, L.; Tylko, J.; Chambers, J.T.; Roberts, T.W.; Church, C.S. Conceptual design of a D8 commercial aircraft. In Proceedings of the 17th AIAA Aviation Technology, Integration, and Operations Conference, Denver, CO, USA, 5–9 June 2017; p. 3590.
53. Rossow, C.C.; von Geyr, H.; Hepperle, M. *The 1g-Wing, Visionary Concept or Naive Solution?* Technical Report DLR-IB-AS-BS-2016-121; DLR: Braunschweig, Germany, 2016.
54. Ma, Y. Design and Optimization for Unconventional Aircraft Configurations with Ultra-High Aspect Ratio Wings. Ph.D. Thesis, TU Braunschweig: Braunschweig, Germany, 2023.
55. Airbus, S. A320-Aircraft Characteristics Airport and Maintenance Planning, 2020. 2019. Available online: [https://aircraft.airbus.com/sites/g/files/jlcpta126/files/2025-01/AC\\_A320\\_0624.pdf](https://aircraft.airbus.com/sites/g/files/jlcpta126/files/2025-01/AC_A320_0624.pdf) (accessed on 20 May 2024).
56. Ma, Y.; Abouhamzeh, M.; Elham, A. Investigating aileron design for ultra-high aspect ratio wings. In Proceedings of the AIAA SCITECH 2023 Forum, National Harbor, MD, USA, 23–27 January 2023; p. 2102.
57. US Department of Defense. *Flying Qualities of Piloted Airplanes MIL-F-8785C*; Technical Report AFWAL-TR-81-3109; AF Wright Aeronautical Laboratories: Wright-Patterson AFB, OH, USA, 1981.
58. Dillinger, J.; Klimmek, T.; Abdalla, M.M.; Gürdal, Z. Stiffness optimization of composite wings with aeroelastic constraints. *J. Aircr.* **2013**, *50*, 1159–1168. [[CrossRef](#)]
59. Elham, A.; van Tooren, M.J. Tool for preliminary structural sizing, weight estimation, and aeroelastic optimization of lifting surfaces. *Proc. Inst. Mech. Eng. Part G J. Aerosp. Eng.* **2016**, *230*, 280–295. [[CrossRef](#)]

**Disclaimer/Publisher’s Note:** The statements, opinions and data contained in all publications are solely those of the individual author(s) and contributor(s) and not of MDPI and/or the editor(s). MDPI and/or the editor(s) disclaim responsibility for any injury to people or property resulting from any ideas, methods, instructions or products referred to in the content.